AGU PUBLICATIONS

JGR

Journal of Geophysical Research: Atmospheres

RESEARCH ARTICLE
10.1002/2016JD026109

Key Points:
- The evaporation from a small lake on the Tibetan Plateau, about 812 mm over the entire ice-free season, is reported for the first time
- U_z has weaker correlation over temporal scales of daily and monthly than half hourly, and ΔE has no contribution under neutral conditions
- The energy budget, with an estimated closure value of 0.97, is generally balanced over the entire ice-free season

Correspondence to:
B. Wang,
wangbinbin@itpcas.ac.cn

Citation:
Wang, B., Y. Ma, W. Ma, and Z. Su (2017), Physical controls on half-hourly, daily, and monthly turbulent flux and energy budget over a high-altitude small lake on the Tibetan Plateau, *J. Geophys. Res. Atmos.*, *122*, 2289–2303, doi:10.1002/2016JD026109.

Received 18 OCT 2016
Accepted 13 FEB 2017
Accepted article online 14 FEB 2017
Published online 28 FEB 2017

Physical controls on half-hourly, daily, and monthly turbulent flux and energy budget over a high-altitude small lake on the Tibetan Plateau

Binbin Wang[1,2,3], Yaoming Ma[1,2,4], Weiqiang Ma[1,2,4], and Zhongbo Su[3]

[1]Key Laboratory of Tibetan Environment Changes and Land Surface Processes, Institute of Tibetan Plateau Research, Chinese Academy of Sciences, Beijing, China, [2]CAS Center for Excellence in Tibetan Plateau Earth Sciences, Chinese Academy of Sciences, Beijing, China, [3]Faculty of Geo-Information Science and Earth Observation, University of Twente, Enschede, Netherlands, [4]University of Chinese Academy of Sciences, Beijing, China

Abstract Precise measurements of evaporation and understanding of the physical controls on turbulent heat flux over lakes have fundamental significance for catchment-scale water balance analysis and local-scale climate modeling. The observation and simulation of lake-air turbulent flux processes have been widely carried out, but studies that examine high-altitude lakes on the Tibetan Plateau are still rare, especially for small lakes. An eddy covariance (EC) system, together with a four-component radiation sensor and instruments for measuring water temperature profiles, was set up in a small lake within the Nam Co basin in April 2012 for long-term evaporation and energy budget observations. With the valuable measurements collected during the ice-free periods in 2012 and 2013, the main conclusions are summarized as follows: First, a bulk aerodynamic transfer model (B model), with parameters optimized for the specific wave pattern in the small lake, could provide reliable and consistent results with EC measurements, and B model simulations are suitable for data interpolation due to inadequate footprint or malfunction of the EC instrument. Second, the total evaporation in this small lake (812 mm) is approximately 200 mm larger than that from adjacent Nam Co (approximately 627 mm) during their ice-free seasons. Third, wind speed shows significance at temporal scales of half hourly, whereas water vapor and temperature gradients have higher correlations over temporal scales of daily and monthly in lake-air turbulent heat exchange. Finally, energy stored during April to June is mainly released during September to November, suggesting an energy balance closure value of 0.97.

1. Introduction

The Tibetan Plateau (TP) is one of the most sensitive areas to climate change and contains tens of thousands of high-altitude lakes. Due to glacier and permafrost melt and increases in precipitation, the total number and area of these high-altitude lakes has increased over time [*Liu et al*., 2010; *Zhang et al*., 2011; *Zhu et al*., 2010]. Because they are considered to be an important indicator of climate change, plateau lakes have been subjected to hydrological analysis. Most previous studies on these lakes have used a combination of conventional meteorological data, remote sensing observations, and model simulations [*Haginoya et al*., 2009; *Lazhu et al*., 2016; *Li et al*., 2001; *Ma et al*., 2016; *Xu et al*., 2009; *Yu et al*., 2011; *Zhu et al*., 2010]. More recently, measurements of eddy covariance (EC) have been made companied by the difficulties associated with the harsh environment, including strong winds, heavy icing, challenging field maintenance, and high financial costs [*Biermann et al*., 2013; *Li et al*., 2015; *Liu et al*., 2014; *Wang et al*., 2015]. These EC measurements provide direct observations of turbulent flux. However, nearly all the lake research that employs EC measurements has focused on large lakes, even though most of the lakes on the Tibetan Plateau are small (98% of the high-altitude lakes smaller than 1 km^2). Thus, long-term EC observations over high-altitude small lakes are needed for understanding turbulent flux interactions between lakes and the atmosphere and informing their roles in local water balance.

As is well understood, latent heat fluxes (*LE*; with *E* as evaporation, in other words) and sensible heat fluxes (*H*) from lakes are primarily controlled by water vapor and temperature gradients, together with turbulent mixing intensity, which is influenced by surface roughness length, wind speed, and atmospheric stability [*Assouline et al*., 2008; *Blanken et al*., 2000; *Blanken et al*., 2011; *Granger and Hedstrom*, 2011; *Heikinheimo et al*., 1999; *Liu et al*., 2012; *Rouse et al*., 2003; *Wang et al*., 2015; *Zhang and Liu*, 2014]. The question of what factors drive turbulent flux exchange between lakes and the atmosphere remains highly relevant. In

addition to the widely observed positive correlations between temperature and water vapor gradients on the one hand and sensible and latent heat fluxes on the other [*Blanken et al*., 2000; *Blanken et al*., 2003; *Liu et al*., 2012; *Liu et al*., 2009; *Liu et al*., 2014; *Zhang and Liu*, 2014], net radiation is an important parameter for estimating evaporation over longer periods, such as 1 day, 10 days, or 1 month [*Rosenberry et al*., 2007; *Yao*, 2009]. However, no clear positive correlations have been observed between net radiation and turbulent heat flux in deep or large lakes [*Blanken et al*., 2000; *Blanken et al*., 2003; *Liu et al*., 2012; *Zhang and Liu*, 2014]. This result contrasts with the positive correlations from shallow lakes over periods longer than a week [*Granger and Hedstrom*, 2011; *Nordbo et al*., 2011]. The reason may be that water surface temperatures in small and shallow lakes respond much faster than those of large or deep lakes to penetration and absorption of solar radiation [*Granger and Hedstrom*, 2011]. For small lakes, a positive correlation is found between wind speed and latent heat flux [*Assouline et al*., 2008; *Granger and Hedstrom*, 2011], while a poor correlation between these factors has been observed for a 0.041 km^2 boreal lake [*Nordbo et al*., 2011]. For large lakes, wind speed has no relationship with latent heat flux at Ross Barnett Reservoir [*Liu et al*., 2012; *Liu et al*., 2009; *Zhang and Liu*, 2014]; however, a positive correlation has been observed for the Great Slave Lake for wind speeds greater than a particular threshold value [*Blanken et al*., 2003]. It has also been found that the presence of unstable (stable) atmosphere boundary layers causes *H* and *LE* to increase (decrease) [*Brutsaert*, 1982]. Another study found that a large upward *LE* persists during periods when the atmosphere is stable [*Heikinheimo et al*., 1999]. Furthermore, *Zhang and Liu* [2014] found that, for Ross Barnett Reservoir, water vapor gradient plays a dominant role in determining energy fluxes under conditions involving large water vapor gradients, while atmospheric stability becomes significant under small water vapor gradients. Therefore, the processes controlling turbulent fluxes between lakes and the atmosphere are likely nonlinear and could be affected by many environmental factors (e.g., temperature and water vapor gradients, wind speed, net radiation, and atmospheric stability) [*Liu et al*., 2012; *Zhang and Liu*, 2014]. There is evidence that large latent heat fluxes (evaporation pulses) could be caused by entrainment of warm, dry air into synoptic weather systems [*Blanken et al*., 2003] or by high-wind events associated with cold fronts [*Liu et al*., 2012; *Liu et al*., 2009], and such pulses have been observed in Lake Ngoring on the TP [*Li et al*., 2015]. Relative to other low-altitude lakes at the same latitude, the solar radiation is high because of a shorter traveling length in the atmosphere and a smaller air density. A predominantly unstable atmosphere is observed in the Nam Co basin [*Biermann et al*., 2013; *Wang et al*., 2015] and Lake Ngoring [*Li et al*., 2015]. Thorough understanding of the physical controls on turbulent flux over high-altitude lakes on the TP is urgently needed.

Evaporation from lakes is a fundamental component of catchment-scale water balance and energy budget analyses [*Rouse et al*., 2005; *Venalainen et al*., 1999; *Zhu et al*., 2010]. Given that they have a lower Bowen ratio (a ratio between *H* and *LE*) and a larger thermal inertia than the surrounding land, lakes favor a lower boundary layer height and increased humidity, which can influence local-scale weather, as well as large-scale circulation patterns [*Nordbo et al*., 2011]. Thus, the responses of lakes to global climate change could be reflected in changes in lake evaporation, which could accelerate climate warming due to increased amounts of water vapor in the atmosphere. Moreover, given that the climate of the TP is changing from cold and dry to warm and wet [*Yang et al*., 2014], precise estimation of evaporation is significant for clarifying the relative importance of local vertical processes and regional horizontal advection as atmospheric moisture sources [*Chen et al*., 2012]. Further, although energy balance is one of the foundations of evaporation simulation and process modeling [*Rosenberry et al*., 2007; *Yao*, 2009], studies of energy budget closure are still scarce [*Gianniou and Antonopoulos*, 2007; *Nordbo et al*., 2011; *Sugita et al*., 2014; *Tanny et al*., 2008], especially on the TP. Estimation of evaporation and the energy budget of high-altitude lakes could provide important information for improving existing models and building new models for simulating these processes.

Lakes, especially small lakes, are sensitive indicators of climate change. The high-altitude lakes of the TP are natural study sites because they have experienced less interference from human activities. Based on a long-term EC monitoring program in a small high-altitude lake within the Nam Co basin during the ice-free periods of 2012 and 2013, our research has two objectives. These objectives are (1) to determine the relative significance of several environmental variables (temperature and water vapor gradients, wind speed, net radiation, and atmospheric stability) on turbulent heat fluxes over temporal scales of half hourly, daily, and monthly and (2) to obtain an assessment of the evaporation and energy balance closure of this small lake. After the materials and methods are introduced in section 2, the results and discussion are presented in section 3. Specifically, section 3.1 discusses the validation of our turbulent heat flux interpolations. Section 3.2.3

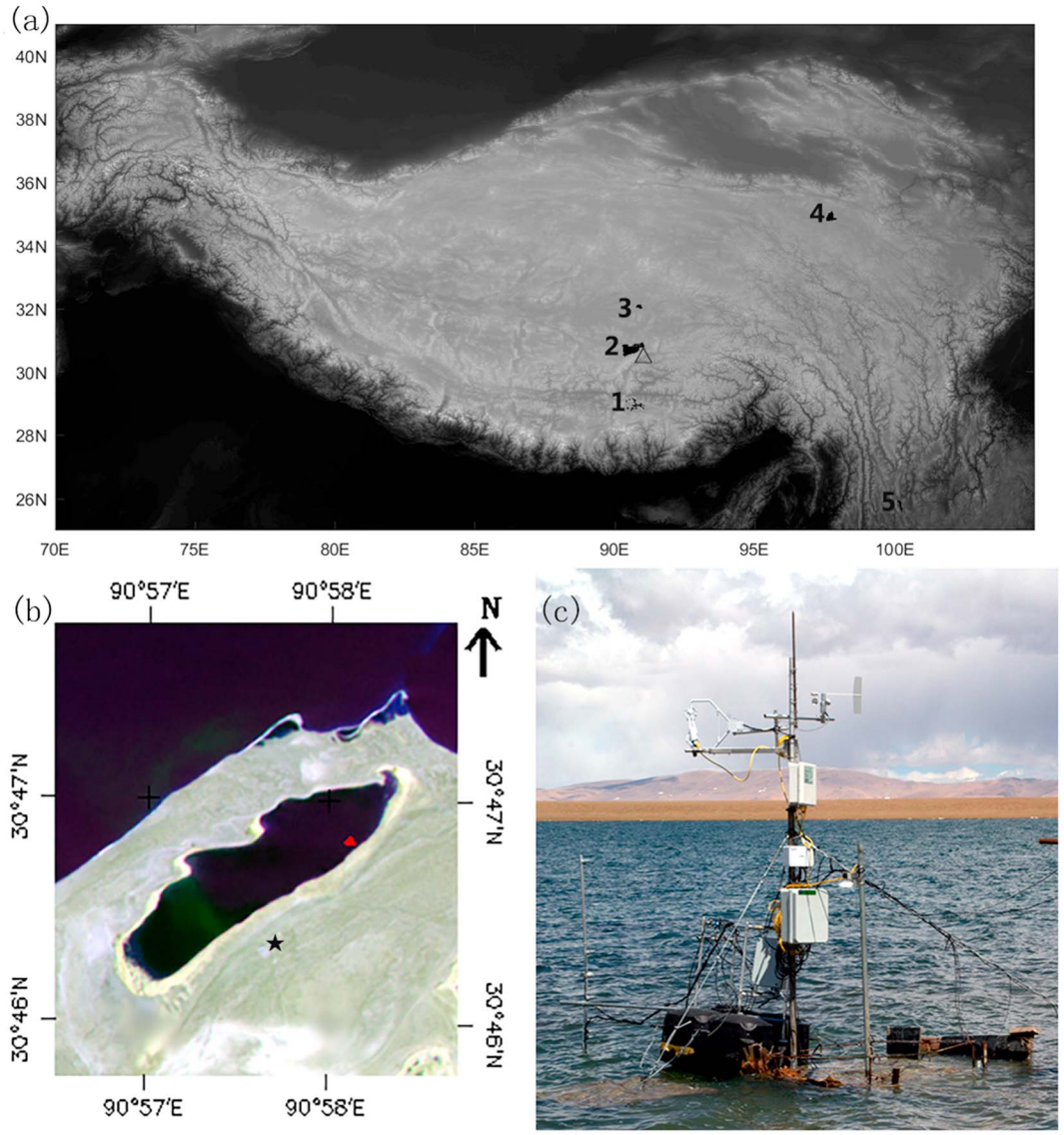

Figure 1. (a) The positions of several high-altitude lakes, with numbers 1–5 indicating the positions of Yamdrok Yum Co, Nam Co, Zige Tang Co, lake Ngoring, and Erhai, respectively; (b) an image of the small lake and the location where field observations were collected; (c) the photo of the instruments.

discusses the observed diurnal variations in turbulent flux and environmental variables and provides a bridge to understanding of the differing physical controls exerted by environmental variables on turbulent heat flux over temporal scales of half hourly (section 3.2.1) and longer (daily and monthly; section 3.2.2). The evaporation and energy budget analysis is discussed in detail in section 3.3. Conclusions are drawn in section 4.

2. Measurements and Methods

The small lake examined in this study (30°46′55″N, 90°58′10″E, 4715 m above sea level, about 1 km^2 with a deepest depth of about 14 m, triangle in Figure 1a) is situated at the southeast edge of the larger lake Nam Co, with only 500 m of land in between (Figure 1b). The study area lies in a transition region between semihumid and semiarid climatic zones and is influenced by the westerly and monsoon systems (May to October). The lake-land breeze provides more precipitation (approximately 500 mm during the monsoon period) because of the small lake's proximity to Nam Co [*Dai et al.*, 2016]. The dominant land cover is an

ecotone composed of alpine meadows and steppe grasses. Since September 2005, the Nam Co Monitoring and Research Station for the Alpine Environment (black star in Figure 1b) has operated an EC system, a planetary boundary layer tower, and a four-component radiation sensor over the grassland for monitoring climatic, meteorological, and environmental changes in the lake basin [*Ma et al*., 2014]. Measurements in Nam Co station provide us a supplemental data for continuous meteorological observations in the small lake. After the short-term lake-air interaction experiment with an EC system in 2010 [*Biermann et al*., 2013], we set up an energy balance system in the small lake (red triangle in Figure 1b) for long-term measurements of evaporation and energy budget analysis. This system, which has been in operation since April 2012, lies 8 m offshore and contains an EC system, radiation sensors, and a temperature profile measurement system that provide direct observations of energy budget components. The instruments shown in Figure 1c include an EC system that is mounted 2.7 m above the water surface, which consists of a three-dimensional sonic anemometer (CSAT3, Campbell Scientific, Inc.) and an open-path CO_2/H_2O infrared gas analyzer (LI 7550, LI-COR, Inc.) for measuring three-dimensional wind speed (U_x, U_y, U_z), temperature (T_a), humidity (q_a), and pressure (P) of the air at 10 Hz. Additionally, a four-component radiation device (CNR4, Kipp & Zonen), 1.5 m above the water surface and toward the south, was used for measuring downward shortwave radiation ($R_{\downarrow}$), downward longwave radiation ($L_{\downarrow}$), upward shortwave radiation ($R_{\downarrow}$), and upward longwave radiation ($L_{\downarrow}$). Twelve temperature sensors are mounted 5 cm, 10 cm, 20 cm, 40 cm, 80 cm, and 160 cm above the water surface and 0 cm, 5 cm, 10 cm, 15 cm, 30 cm, and 60 cm below the water surface. These temperature sensors are fixed in a vertical pipe to prevent direct Sun exposure. The water surface temperature (T_s) is obtained from the sensor closest to the water surface. All the instruments are powered by two 80 W solar panels. Data are stored in a data logger (CR5000, Campbell Scientific, Inc.) and retrieved monthly.

The energy budget of a lake indicates that the incoming energy is balanced by outgoing energy and energy stored in water [*Gianniou and Antonopoulos*, 2007; *Tanny et al*., 2008], and it can be expressed as equation (1).

$$R_n = H + LE + G_s + G_b + G_a \tag{1}$$

where net radiation (R_n, W m^{-2}) is the sum of $R_{\downarrow}$, $L_{\downarrow}$, $R_{\downarrow}$ reflected by the water surface, and $L_{\downarrow}$ reflected and emitted by the water surface. R_n is balanced by the sensible heat flux (H, W m^{-2}), the latent heat flux (LE, W m^{-2}), the heat storage change in the water (G_s, W m^{-2}), the heat transfer between water and the bottom sediments (G_b, W m^{-2}), and the net energy (G_a, W m^{-2}) gained or lost by the lake due to the exchange of water masses resulting from the inflow-outflow balance. As there is no surface inflow or outflow and there are no observations describing the heat transfer between water and sediments, G_a and G_b are omitted in energy budget analysis.

H and LE are obtained through the eddy covariance method using the "Turbulence Knight 3" software package (https://zenodo.org/record/20349#), and all relevant corrections (including time lag compensation, spike removal, planar fit rotation, spectral correction, and Webb-Pearman-Leuning density correction) are performed in the processing of high-frequency data [*Mauder and Thomas*, 2015]. Moreover, planar fit rotation, including data only from the direction of the lake, is performed to correct for the influence of the terrain structure of the bank [*Biermann et al*., 2013]. A footprint analysis shows that turbulent flux observations from the direction of the lake could represent lake-air interactions [*Biermann et al*., 2013; *Wang et al*., 2015]. Observations with poor data quality or those contaminated by land are interpolated using bulk aerodynamic transfer model (B model) simulations [*Verburg and Antenucci*, 2010; *Wang et al*., 2015]. The input variables of B model are traditional meteorological variables (T_s, T_a, q_a, U_z, and P), and the output variables are lake-air heat fluxes (H and LE) and friction velocity (U_*). The estimation methods are mainly expressed as equations (2) and (3):

$$H = \rho_a c_p C_H U_z (T_s - T_a) \tag{2}$$

$$LE = \rho_a L_v C_E U_z (q_s - q_a) \tag{3}$$

where ρ_a is the air density (kg m^{-3}); c_p is the specific heat of air (1005 J kg^{-1} K^{-1}); L_v is the latent heat of vaporization (J kg^{-1}); U_z (m s^{-1}) is the wind speed at the reference height (Z = 2.7 m); T_a (K) and q_a (kg kg^{-1}) are the temperature and specific humidity at the reference height, and T_s (K) and q_s (kg kg^{-1}) are the same quantities at the water surface; and C_H and C_E are the bulk transfer coefficients for heat and water, respectively. The bulk transfer coefficients, assumed to be equal in B model, are related to atmospheric stability ($\zeta = Z/L$) and roughness length for momentum (z_{0m}), where $z_{0m} = \alpha \frac{U_*}{g} + R_r \frac{v}{U_*}$, L is Monin-Obukhov length, U_* is friction velocity

($m\,s^{-1}$), ν is kinematic viscosity of air ($m^2\,s^{-1}$), and g is gravitational acceleration ($m\,s^{-2}$). The Charnock number ($\alpha = 0.031$) and roughness Reynolds number ($R_r = 0.54$) are optimized considering the specific wave effect of the small lake. Further details of the site, the EC data processing methods, the B model, and parameters optimization of the B model can be found in *Wang et al.* [2015].

Heat storage change in the water can be obtained from lake temperature profiles [*Blanken et al.*, 2000; *Nordbo et al.*, 2011]. The heat storage change (G_s) of the lake at a given depth (z, m) over a given time interval (Δt, s) can be calculated using equations (4) and (5):

$$G_s = \rho_w c_{pw} \frac{\overline{\Delta T_w}}{\Delta t} z \tag{4}$$

$$\overline{T_w} = \frac{1}{z} \sum_{i=1}^{n} T_{wi} \Delta z_i \tag{5}$$

$$G_c = \rho_w c_{pw} \left(\overline{T_w} - T_r\right) z \times 10^{-6} \tag{6}$$

where ρ_w ($g\,m^{-3}$) and c_{pw} ($J\,kg^{-1}\,K^{-1}$) are the density and specific heat of water, respectively; $\overline{T_w}$ (K) is the mean water temperature; and T_{wi} (K) and Δz_i (m) are the water temperature and the representative thickness of layer i (from *1* to n). When the reference temperature (T_r, K) is taken to represent an ice-water mixture with a value of 0°C and is used as the origin, the cumulative water heat storage (G_c, $MJ\,m^{-2}$) can be expressed through equation (6). Due to the freezing and thawing processes, the temperature sensors in the water were all destroyed in April 2013. Because of the importance of surface water temperature changes caused by surface warming and cooling [*Fairall et al.*, 1996], one temperature sensor in the air was used to measure the T_s of the water. Except for that, the temperature profiles did not function during 16 May to 6 July in 2012. Thus, considering the wave effects, lake-level variations (less than 20 cm), and strong mixing in the water surface layer, two representative temperatures, one close to the water surface and one at a depth of 60 cm, are chosen to represent the shallow mixing layer and "deep layer," with thicknesses of 0.3 m and 0.7 m, respectively. If the temperature at 60 cm was not available, only the temperature close to the water surface was used, representing a thickness of 1 m. The total calculated depth is 1 m if no further information is given.

To describe the similarity of variations between environmental variables and H and LE, the Fréchet distance [*Alt and Godau*, 1995] and the root-mean-square error (RMSE) are used to measure differences among selected pairs of normalized variables. All the variables (H, LE, $U_z\Delta T$, $U_z\Delta E$, U_z, ΔT, ΔE, ζ, and R_n) are normalized to the range [0, 1] using the largest and smallest values from time series representing half-hourly, daily, and monthly data. The normalization equation is $\mathrm{Out}_i = \frac{\mathrm{In}_i - \mathrm{In}_{\min}}{\mathrm{In}_{\max}}$, where In is the original data set and Out is the normalized data set, where $\mathrm{In}_{\min}$ is the minimum, $\mathrm{In}_{\max}$ is the maximum, In_i is a specific value at position i for half-hourly, daily, or monthly data series. A small Fréchet distance or low RMSE values indicate high similarity between two curves. In addition, the mean bias (MB), Pearson's correlation coefficient (R), and coefficient of determination (R^2) are also used for mathematical evaluation [*Wang et al.*, 2015].

3. Results and Discussion

3.1. Heat Flux Interpolation

The B model, which is optimized for the specific wave pattern of the small lake [*Wang et al.*, 2015], is chosen for half-hourly data interpolation to fill gaps due to instrument failure or inadequate footprint and quality. The B model was optimized using observations from 2012 (Figures 2a–2c) and was further validated independently for observations from 2013 (Figures 2d–2f). The correlation coefficients (0.87 and 0.83) and the slopes of lines of best fit that pass through the origin (1.03 and 0.91) in 2012, which could describe the relationship between simulated and observed H and LE values, are very close to those (0.84 and 0.82; 1.05 and 0.92) from data in 2013. Therefore, the B model with tuned parameters is appropriate for data interpolation over periods with low-quality or missing observations. However, overestimation in simulated H (for which the slope of the line of best fit is larger than 1) and underestimation in simulated LE (for which the slope of the line of best fit is smaller than 1) is found, and it results from the differences in observed roughness lengths for heat and for water, which are considered same in the B model simulations [*Wang et al.*, 2015]. The MB values are corresponding to the overestimation of simulated H and underestimation of simulated LE at monthly scales (Table 1). The monthly averaged heat flux could be corrected by mean MB values, which were $-2.2 \pm 1.1\,W\,m^{-2}$ for simulated H and $11.2 \pm 3.7\,W\,m^{-2}$ for simulated LE, respectively. In addition, the

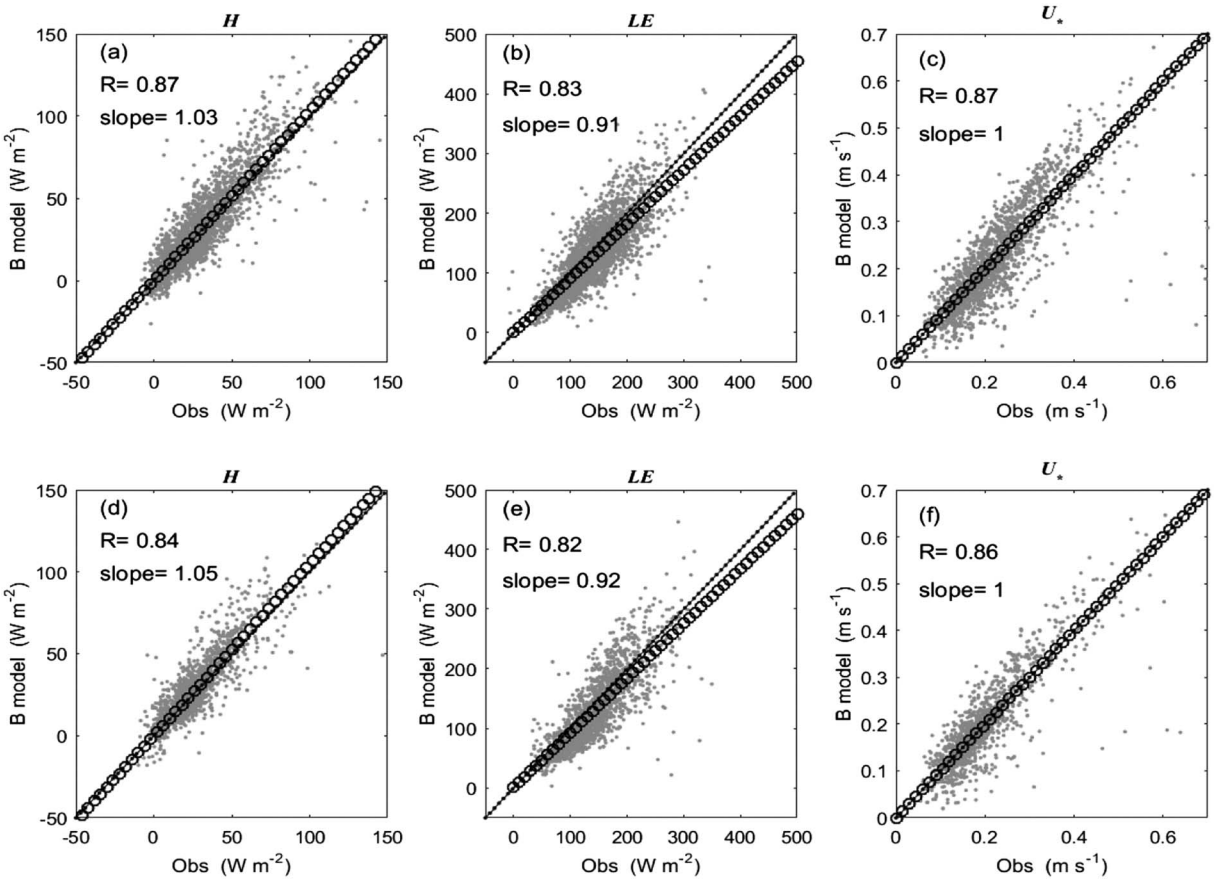

Figure 2. Scatterplots of *H*, *LE*, and U_* between B model simulations and observations (Obs) in (a–c) 2012 and in (d–f) 2013. Lines drawn with dots and circles represent the 1:1 line and the line of best fit, respectively. Correlation coefficients (*R*) and the slope of the line of best fit (passing through the origin) are indicated.

simulated monthly *H* and *LE* values follow the observations well, and the values with MB corrections are much closer to the observations.

3.2. Environmental Controls on *H* and *LE* Over Different Temporal Scales

3.2.1. Environmental Controls on Turbulent Flux Over Half-Hourly Scales

Relative to other single environmental variables, wind speed (U_z) has the most significant contribution to variation of half-hourly *H* ($R^2 = 0.4$) and *LE* ($R^2 = 0.48$), as shown in Figure 3 and Table 2. With a relatively high correlation value of ΔT ($R^2 = 0.38$), the product ($U_z\Delta T$, $R^2 = 0.77$) of ΔT and U_z determines the variation in *H*. Even though the correlation between ΔE and *LE* is weak ($R^2 = 0.1$), the product of ΔE and U_z enhance the correlations between *LE* and $U_z\Delta E$ ($R^2 = 0.67$) significantly. Due to the penetrating and absorbing of solar radiation in the water, R_n is considered to have no obvious correlations with half-hourly *H* and *LE* [*Zhang and Liu*, 2014], and this hypothesis is also supported by our observations (H_R_n, $R^2 = 0.06$; LE_R_n, $R^2 = 0.03$). The atmospheric stability (ζ, $R^2 = 0.005$) has no correlation with *H*, while its correlation ($R^2 = 0.17$) with *LE* is even higher than

Table 1. MB Values of Monthly Average *H* and *LE* Between Observations and Simulations in 2012 and 2013[a]

Year	Unit: W m^{-2}	April	May	June	July	August	Mean	SD
2012	*H*	−3.4	−2.6	−0.9	−1.9	−1.1	−2.0	1
	LE	14.2	7.3	7.7	14.4	11.1	10.9	3.4
2013	*H*	----	−2.2	−2.7	−3.5	−0.7	−2.3	1.2
	LE	----	10.5	15.5	6.2	13.4	11.4	4.0

[a]SD: standard deviation.

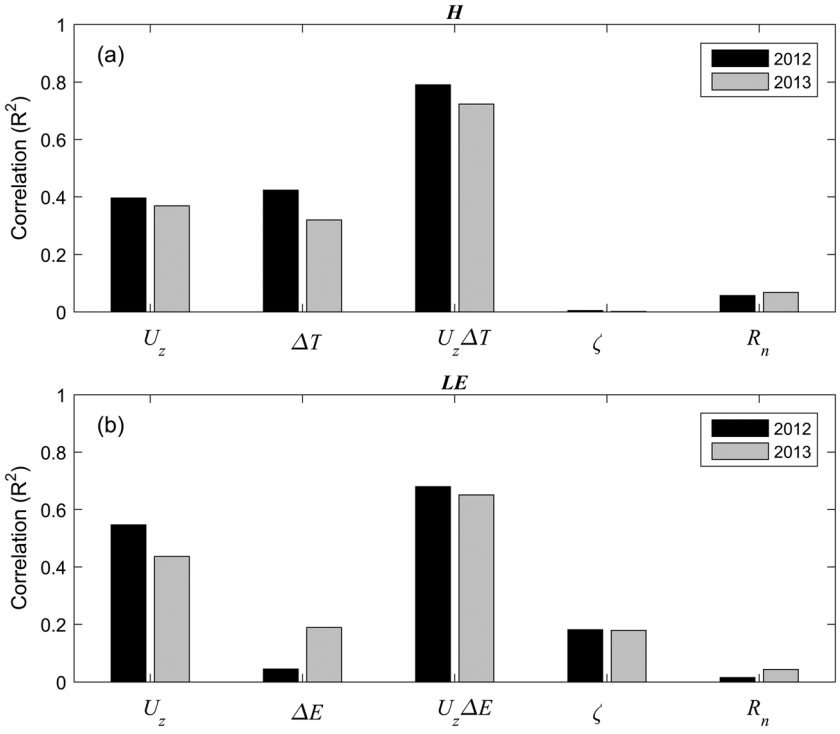

Figure 3. The coefficients of determination (R^2) between half-hourly (a) *H*, (b) *LE*, and meteorological variables in 2012 and 2013, respectively.

that of ΔE. The strong correlations between ζ and *LE* corresponds to the fact that *LE* increase from "extremely unstable" conditions and achieve its largest value at "neutral" conditions (Figure 4e).

As the correlations between ζ and *H* and *LE* are highly nonlinear [*Zhang and Liu*, 2014], variations of *H*, *LE*, and environmental variables are grouped at different atmospheric stability bins (extremely unstable [−10, −1], "unstable" [−1, −0.5], "weakly unstable" [−0.5, −0.1], "near neutral" [−0.1, −0.05], neutral, [−0.05, 0.05]) in Figure 4, with coefficients of determination calculated at each bin. Obviously, *H* increases from extremely unstable atmosphere, peaks at near-neutral conditions, and then decreases in neutral conditions (Figure 4a). And it is near zero or negative under stable conditions (only a few observations were obtained, which are not shown). $U_z\Delta T$ has the largest correlation with *H* in different atmospheric stability bins (Figure 4d). ΔT has relatively higher coefficients of determination than U_z under extremely unstable and unstable conditions,

Table 2. Coefficients of Determination (R^2) Between *H* and *LE* and Environmental Variables for 2012, 2013, and Both Years Together

(R^2)	Temporal scales	2012	2013	All	(R^2)	Temporal scales	2012	2013	All
H_U_z	30 min	0.40	0.37	0.40	LE_U_z	30 min	0.55	0.44	0.48
	Daily	0.11	0.04	0.06		Daily	0.34	0.14	0.24
	Monthly	0.17	0.58	0.20		Monthly	0.51	0.33	0.18
$H\_\Delta T$	30 min	0.42	0.32	0.38	$LE\_\Delta E$	30 min	0.04	0.19	0.10
	Daily	0.56	0.74	0.66		Daily	0.48	0.66	0.56
	Monthly	0.61	0.95	0.71		Monthly	0.85	0.95	0.88
$H\_U_z\Delta T$	30 min	0.79	0.72	0.77	$LE\_U_z\Delta E$	30 min	0.67	0.66	0.67
	Daily	0.86	0.90	0.87		Daily	0.92	0.92	0.92
	Monthly	0.94	0.93	0.91		Monthly	0.97	0.99	0.97
H_ζ	30 min	0.005	0.002	0.005	LE_ζ	30 min	0.18	0.18	0.17
	Daily	0.002	0.01	0.005		Daily	0.39	0.15	0.27
	Monthly	0.06	0.21	0.05		Monthly	0.77	0.22	0.59
H_R_n	30 min	0.06	0.07	0.06	LE_R_n	30 min	0.02	0.04	0.03
	Daily	0.09	0.23	0.17		Daily	0.08	0.34	0.19
	Monthly	0.27	0.97	0.58		Monthly	0.08	0.68	0.36

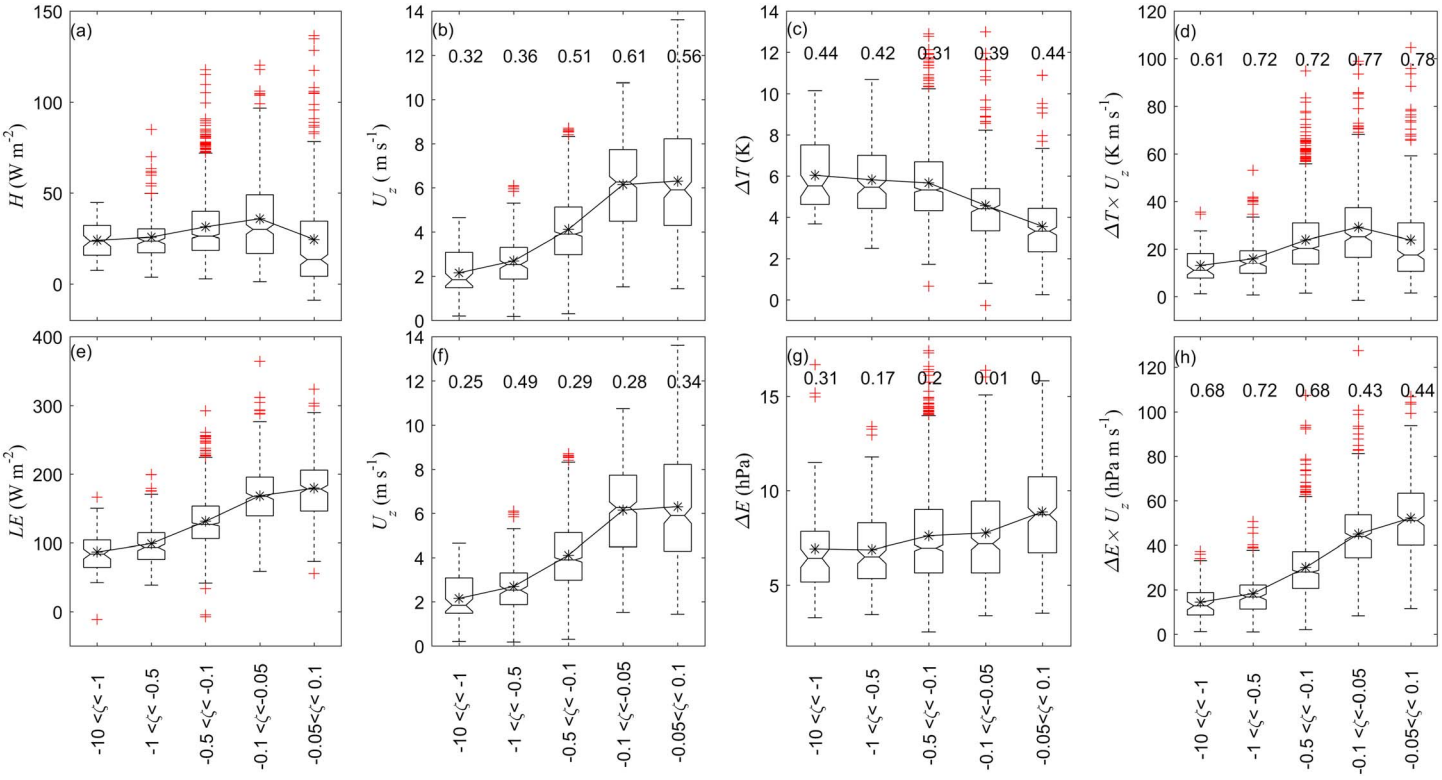

Figure 4. Box plots of (a) H, (b) U_z, (c) ΔT, (d) $U_z\Delta T$, (e) LE, (f) U_z, (g) ΔE, and (h) $U_z\Delta E$ in different stability bins. The average value of each variable in each stability bin is plotted as an asterisk, and the coefficients of determination (R^2) for the stability bins are given in Figures 4b–4d and Figures 4f–4h, respectively.

while under weakly unstable to neutral conditions, U_z, rather than ΔT, is more strongly correlated with H (Figures 4b and 4c). Additionally, ΔT shows relatively stable correlations with H ($R^2 = 0.4$), while the correlations between U_z and H increase from extremely unstable condition to neutral conditions (R^2 changes from 0.32 to approximately 0.6). Therefore, we conclude that the transport mechanism of H at half-hourly scales has a stable effect through ΔT, while the transport efficiency (U_z) shows increasing significance with increased U_z. For LE, $U_z\Delta E$ describes such variations and has the best correlations under all atmospheric conditions (Figure 4h). The coefficients of determination for U_z are all larger than 0.25 (Figure 4f), while ΔE displays relatively larger correlations under unstable conditions but has values close to 0 at near-neutral and neutral conditions (Figure 4g). Thus, it is concluded that U_z makes a relatively significant contribution to LE, while ΔE is only important under unstable atmospheric conditions (with smaller wind speeds and larger temperature gradients).

3.2.2. Environmental Controls on Turbulent Flux Over Daily and Monthly Scales

On daily scales, the daily average T_s and vapor pressure (E_s) at the water surface are larger than the daily average T_a and vapor pressure (E_a) in the air (Figures 5g and 5h). Thus, the positive daily average ΔT (6.31 K) and ΔE (686.9 Pa) indicate that large amounts of heat are released through H and LE, and the average values of H and LE are 33.3 W m^{-2} and 112.8 W m^{-2}, respectively, for the summer ice-free period. H is largest during periods with larger ΔT, while LE is larger during the months when ΔE is larger (Figures 5a−5d). The most obvious evidence for the influence of ΔT on H is seen around November 2013, when large values of H coincide with large ΔT values; while in both June 2012 and June 2013, the variations in LE clearly parallels similar variations in ΔE. Meanwhile, there also exists an average wind speed of 3.46 m s^{-1} (Figure 5e), and the atmosphere is always in an unstable condition (Figure 5f) due to the large ΔT and ΔE.

Of all the single meteorological variables as shown in Table 2, ΔT and ΔE show the best correlations with H and LE for daily and monthly scales. In contrast, U_z has relatively small correlations with H and LE at daily and monthly scales; however, the contribution from U_z cannot be ignored. It could increase the

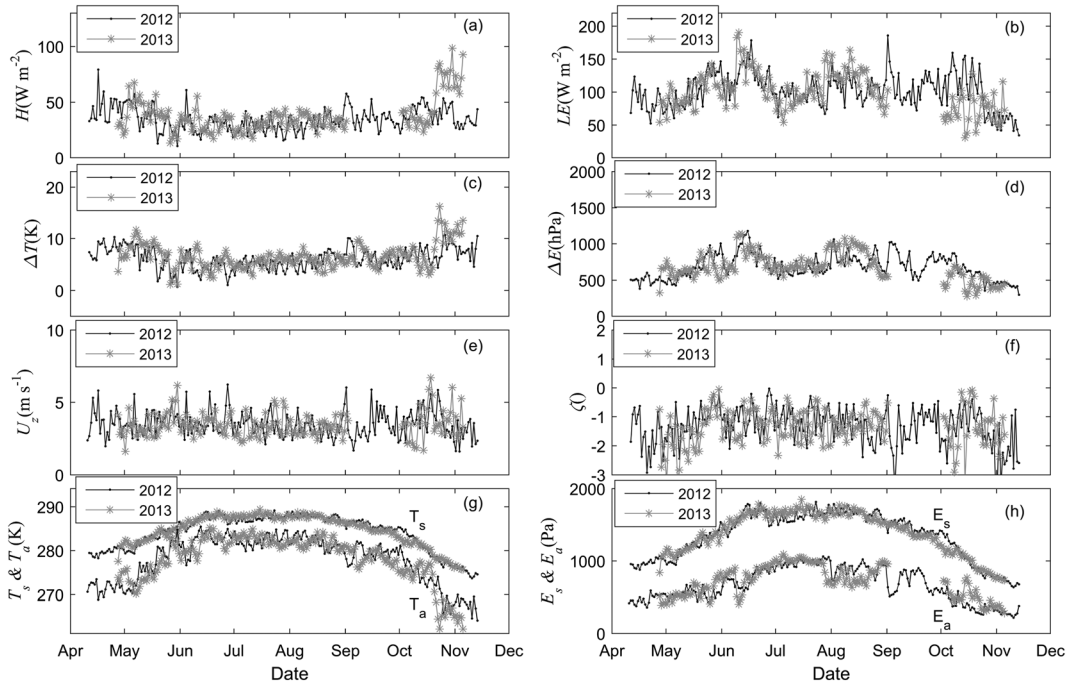

Figure 5. Variation of daily (a) H, (b) LE, (c) ΔT, (d) ΔE, (e) U_z, (f) ζ, (g) T_s and T_a, and (h) E_s and E_a in ice-free periods of 2012 and 2013.

correlations of both H and $U_z\Delta T$ and LE and $U_z\Delta E$ significantly, so that they are all larger than 0.87. In addition, ΔE in November of 2012 is larger than that in 2013; however, larger values of LE are observed in 2013 with greater contributions from U_z, as shown in Table 4. Thus, cold fronts [*Liu et al*., 2009] and entrainment of dry air [*Blanken et al*., 2003], together with the effects of high winds, are considered to be evaporation pulse events, which are thought to increase evaporation through large U_z and large ΔE. Atmospheric stability is almost uncorrelated with H, while the coefficient of determination between LE and atmospheric stability is 0.27 for daily scale and 0.59 for monthly scale. R_n has a negative correlation with H ($R^2 = 0.17$), which reflects the phenomenon of observed larger temperature gradient during low-temperature periods (i.e., at night or during cool seasons). And R_n has a weak positive correlation with LE, as in *Granger and Hedstrom* [2011] and *Nordbo et al*. [2011]. Moreover, U_z shows relatively larger correlations at half-hourly scale than at daily and monthly scales. Meanwhile, the correlation coefficients increase from half-hourly scales to monthly scales for ΔT ($U_z\Delta T$) and ΔE ($U_z\Delta E$). Atmospheric stability and net radiation have better correlations for H and LE, respectively, at daily and monthly scales than at half-hourly scales.

3.2.3. Diurnal Variation of Turbulent Flux and Environmental Variables

H has relatively higher values at night than during the day, similar to the diurnal variation in ΔT (Figures 6a and 6c). LE has relatively high values in the afternoon, which is similar to the variation in the ΔE (Figures 6b and 6d). As shown in Figure 6, U_z has a clear influence on the average diurnal variation in H and LE, where two peak values are clearly observed at 3:30 and 8:00 in U_z, $U_z\Delta E$, $U_z\Delta T$, H, and LE. We deduce that the large latent heat fluxes are caused by coupling effect between U_z and ΔE, with a higher contribution from U_z at night and a higher contribution from ΔE during the day. Moreover, ΔT and ΔE determine the average diurnal variation in H and LE, while U_z adjusted the magnitudes of these fluctuations. Fréchet distances and RMSE values calculated for normalized H, LE, and all the environmental variables over diurnal, daily, and monthly scales are shown in Table 3. Similar as the previous results, the variation of diurnal, daily, and monthly values of $U_z\Delta T$ and $U_z\Delta E$ have the smallest Fréchet distances and RMSE values with H and LE, respectively. The variation in ΔE is much more similar to the variation in LE than that in U_z at diurnal, daily, and monthly scales. Similarly, the variation in ΔT has a closer similarity with H than that in U_z at daily and monthly scales, with an opposite result at diurnal variations, which may indicate the effect of lake-land breeze circulation. Moreover, atmospheric stability has the least similarity for H and LE with only an exception with LE on monthly scales.

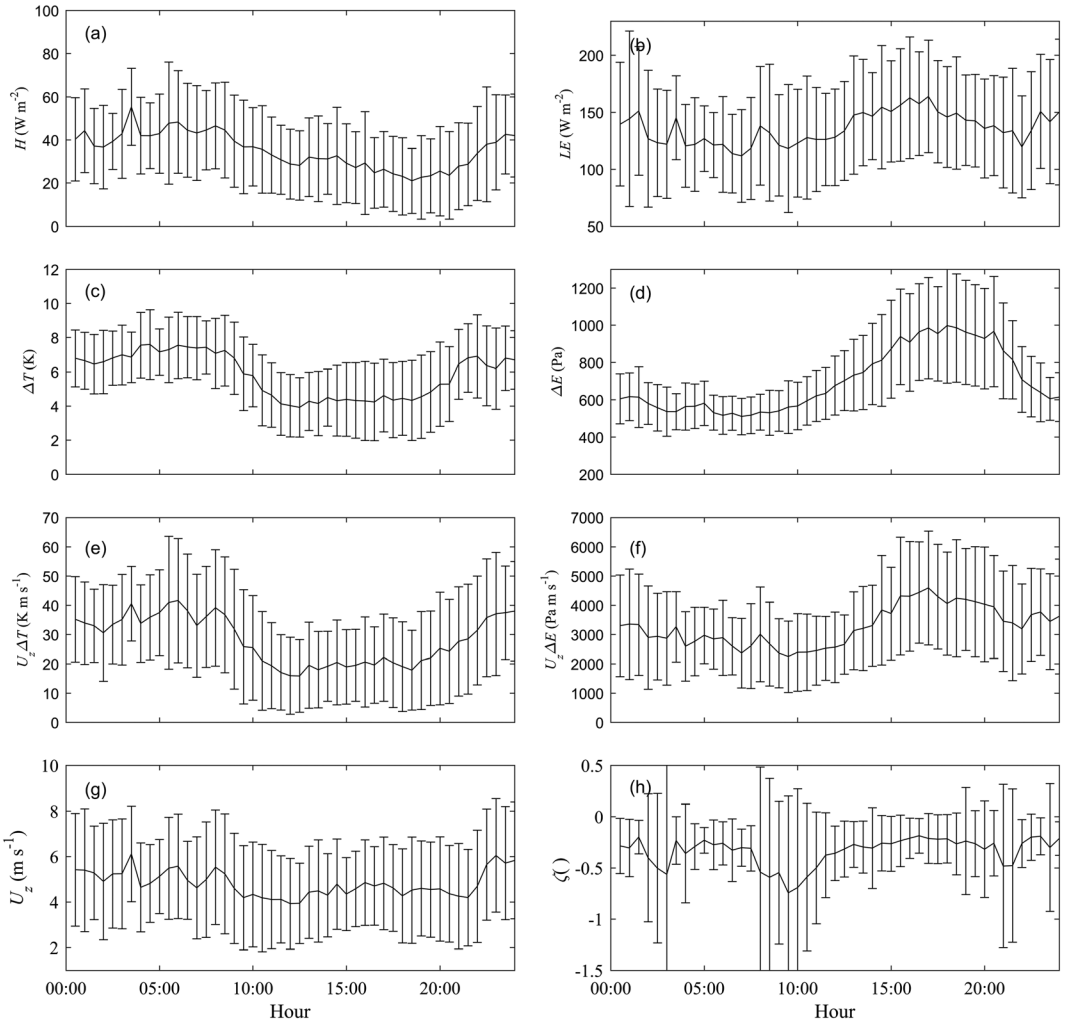

Figure 6. Averaged diurnal variation of (a) H, (b) LE, (c) ΔT, (d) ΔE, (e) $U_z\Delta T$, (f) $U_z\Delta E$, (g) U_z, and (h) ζ during the ice-free period in 2012. Error bars are shown.

3.3. Analysis of Energy Budget and Evaporation

3.3.1. Energy Budget

During the ice melt period, water and ice are mixed with all the energy used for phase transition, and the temperature at 0°C is considered as a reference for the cumulative heat storage (G_c) calculation. The variation in G_c, the relationship between "daily residual heat" (defined as $(R_n)_i - H_i - LE_i$ here) and daily water heat storage (G_{si}), and the variation in daily residual heat and temperature difference of pairs of consecutive days (ΔT_i) are shown in Figure 7. Generally, the lake gains heat from April to June and releases it mainly through October (Figure 6a), when turnover may speed up the heat release process as in *Nordbo et al.* [2011]. G_c achieves a maximum value of approximately 65 MJ m^{-2} in both 2012 and 2013. This value is smaller than that from a 0.041 km^2 lake Valkea-Kotinen [*Nordbo et al.*, 2011],

Table 3. The Fréchet Distances (FD) and RMSE Values Between Important Environmental Variables and H and LE[a]

	Diurnal		Daily		Monthly	
	FD	RMSE	FD	RMSE	FD	RMSE
$H\_U_z\Delta T$	1.2	0.17	1.4	0.07	0.23	0.11
$H\_\Delta T$	1.6	0.23	2.2	0.11	0.30	0.15
H_U_z	1.3	0.19	4.1	0.21	0.46	0.33
H_ζ	3.4	0.49	8.0	0.41	0.77	0.45
$LE\_U_z\Delta E$	1.1	0.16	1.3	0.07	0.17	0.09
$LE\_\Delta E$	1.8	0.26	2.6	0.13	0.40	0.16
LE_U_z	2.4	0.35	3.7	0.19	0.54	0.46
LE_ζ	2.5	0.49	4.9	0.25	0.48	0.39

[a]All the variables are normalized to the range [0, 1].

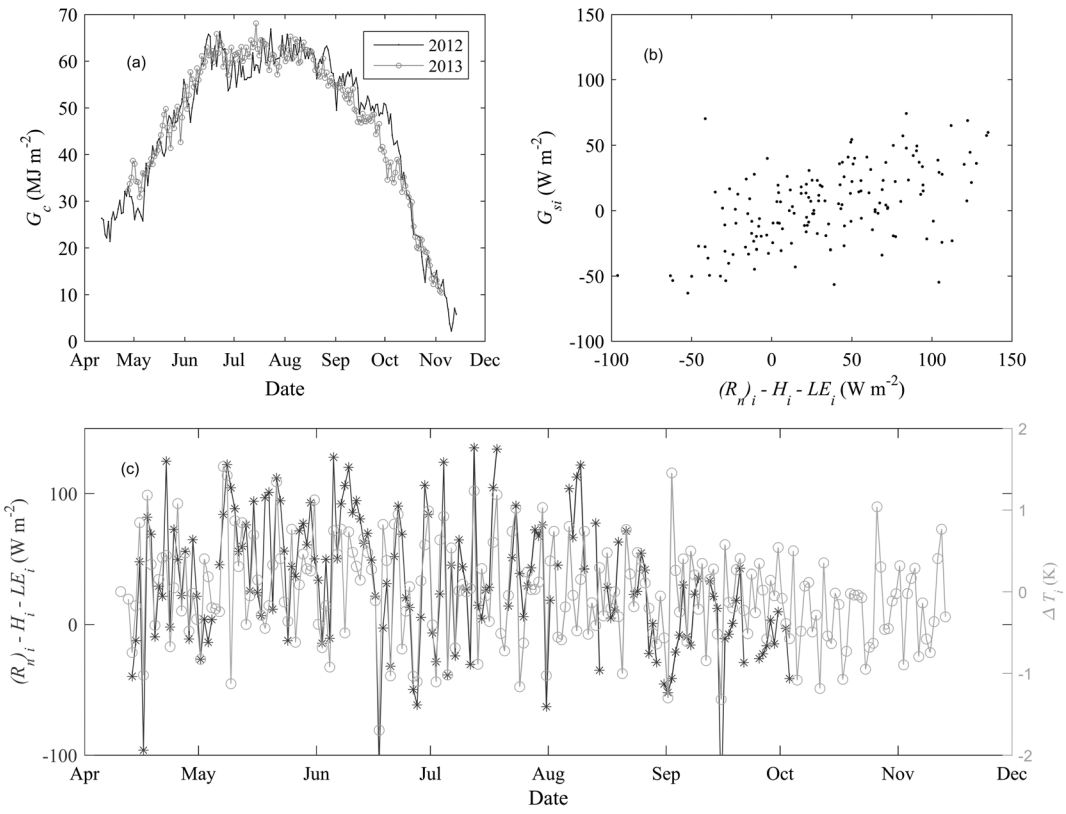

Figure 7. (a) Variation in G_c in 2012 and in 2013; (b) relationship between daily water heat flux (G_{si}) and $(R_n)_i - H_i - LE_i$ at day i over the ice-free period of 2012; (c) variation in $(R_n)_i - H_i - LE_i$ and ΔT_i in 2012.

which has a higher average temperature at 1 m depth. The daily residual heat has a positive correlation coefficient ($R = 0.6$) with the total G_{si} (Figure 6b). However, it should be noted that daily residual heat is calculated by averaged half-hourly data, while G_{si} is the daily total stored heat at 1 m depth in the water. Moreover, the variation in daily residual heat corresponds well with the variation in ΔT_i (Figure 7c), and the observation that positive (negative) residual heat corresponds to lake temperature increase (decrease) justifies our observations. The variation in G_c also indicates that heat release (accumulation) could also occur during periods when heat is stored (released). The average energy balance closure (EBC), considering temporal scales of daily, from 10 April 2012 to the end of September 2012 is approximately 0.836.

The diurnal cycle of monthly average R_n peaks at solar noon (approximately 14:00 GMT +8) and is negative at night, with values ranging from 800 W m^{-2} to −130 W m^{-2} (Figure 8a). R_n is generally larger than that from a low-altitude lake [*Liu et al.*, 2012] with similar latitude. The diurnal cycles of G_s behaved similarly to net radiation, with earlier peaks due to the occurrence of the largest temperature increases at approximately 12:00 (GMT +8) in Figure 8b. The values, with deep layer included, ranged from approximately 370 W m^{-2} (in April) to −300.0 W m^{-2} (in November), and most of the energy gained during the day was released at night. Moreover, G_s obtained through surface temperature (one close to the water surface) has a much larger amplitude than that through two temperatures (one close to the water surface and one at 60 cm), i.e., July and August in 2012 and 2013. However, this difference is quite small during heat releasing period in September and October. G_s fuels the nighttime turbulent fluxes, where significant nocturnal *LE* and *H* are present. *H* generally reaches its minimum value in the afternoon and its maximum value in the early morning (Figure 8d), with similar diurnal variations as in the temperature gradient [*Liu et al.*, 2012]. The different shape of *H* in April was influenced by U_z, with relatively small values at night and relatively large values during the day; these values ranged from 15 W m^{-2} to 55 W m^{-2}. Diurnal cycles of *LE* achieve their maximum values in the afternoon (18:00 GMT +8), while the minimum values occur at night (Figure 8c).

The average energy balance closure (EBC) is 0.93 during part of the whole open-water period (from 10 April to 31 October) with values falling between a minimum of 0.78 in May and a maximum of 1.57 in October

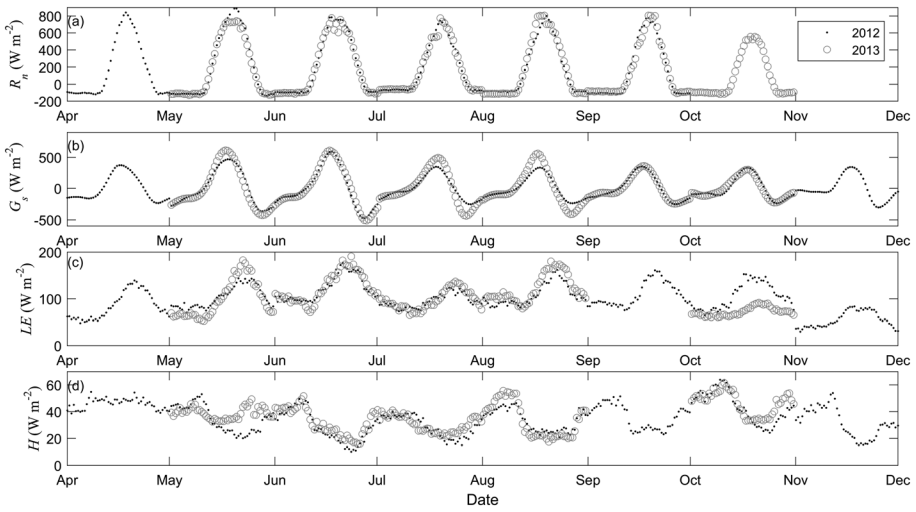

Figure 8. Monthly averaged diurnal cycles of (a) net radiation (R_n), (b) water heat storage (G_s), (c) latent heat flux (LE), and (d) sensible heat flux (H) in 2012 and 2013.

(Table 4). Most of the energy absorbed in April to June is released during September to November, whereas the water storage in July and August is relatively small. If the unavailable net radiation in November were to have a value of 50 W m^{-2}, the EBC value would be much closer to 1 (0.97). The EBC value is generally high compared with the results of other energy budget studies [*Nordbo et al*., 2011]. The EBC value is supported by the following reasons: the turbulent fluxes are based on eddy covariance measurements; observations that are contaminated by inadequate footprint, bad data quality, or instrument errors are suitably

Table 4. Monthly Averaged Environmental Variables and Heat Fluxes During the Open-Water Period in 2012 and 2013 and Averages of the 2012 and 2013 Values (Ave)[a]

		April	May	June	July	August	September	October	November
ΔT (K)	2012	8.09	5.95	4.60	5.04	5.89	6.19	7.24	7.54
	2013	------	7.27	5.59	5.35	5.65	6.54	7.96	11.61
	Ave.	8.09	6.61	5.10	5.20	5.77	6.37	7.6	9.58
ΔE (Pa)	2012	498.7	669.6	830.7	645.0	778.5	760.1	628.5	430.6
	2013	------	648.0	815.0	707.7	844.2	548.6	482.0	396.1
	Ave.	498.7	658.8	822.9	676.4	811.4	654.4	555.3	413.4
U (m s^{-1})	2012	3.59	3.64	3.65	3.43	3.21	3.41	3.79	2.79
	2013	------	3.53	3.50	3.32	3.24	3.95	3.62	3.14
	Ave.	3.59	3.59	3.58	3.38	3.23	3.68	3.71	2.96
ζ ()	2012	−1.65	−1.16	−1.06	−1.06	−1.35	−1.37	−1.38	−2.25
	2013	------	−1.54	−1.18	−1.31	−1.24	−0.52	−1.34	−1.81
	Ave.	−1.65	−1.35	−1.12	−1.19	−1.30	−0.95	−1.36	−2.03
H (W m^{-2})	2012	43.6	32.3	26.6	26.6	31.2	33.9	41.2	29.6
	2013	------	36.6	29.7	28.3	31.5	----	44	----
	Ave.	43.6	34.5	28.2	27.5	31.4	33.9	42.6	29.6
LE (W m^{-2})	2012	96	114	132.9	105.6	119.1	119.9	116.6	64.9
	2013	------	109.3	134.8	107.8	132.1	----	83.4	66.5
	Ave.	96	111.7	133.9	106.7	125.6	119.9	100	65.7
G_s (W m^{-2})	2012	10.6	4.9	6.9	0.6	0.6	−3.3	−8.8	−8.2
	2013	10.6	5.3	6.8	1.1	−0.7	−4.0	−8.2	−5.9
	Ave.	10.6	5.1	6.9	0.8	−0.04	−3.7	−8.5	−7.0
R_n (W m^{-2})	2012	161.8	202.1	200.5	167.8	167.4	143.3	----	----
	2013	----	182.4	193.0	170.3	177.6	----	82.1	----
	Ave.	161.8	192.3	196.8	169.1	172.5	143.3	82.1	----
EBC	Ave.	0.92	0.78	0.85	0.80	0.91	1.05	1.57	----

[a]A lake depth of 2 m is assumed for G_s here.

Table 5. Evaporation From High-Altitude Lakes on the Tibetan Plateau[a]

	Area; Depth; Altitude; Ice-Free Period	Year	Methods	$\bar{E}$ (mm)	E (mm)	Reference
Nam Co	2000 km^2; 40 m; 4730 m; Jun–Jan	1979–2012	CRLE	----	635 Jun–Jan	*Ma et al.* [2016]
Nam Co	ibid.	1979–2014	Flake model	832	642[b] Jun–Jan	*Lazhu et al.* [2016]
Nam Co	ibid.	1961–2005	Bulk method	621	----	*Xu et al.* [2009]
Nam Co	ibid.	2006–2008	Bulk method	658	603 Jun–Jan	*Shigenori et al.* [2009]
Yamdrok Yum Co	638 km^2; 20–40 m; 4441.5 m; Apr–Nov	1961–2005	Bulk method	1252	830 Apr–Nov	*Yu et al.* [2011]
Ngoring	610 km^2; 17 m; 4274 m; Apr–Nov	2011–2012	EC	----	436 Jun–Nov	*Li et al.* [2015]
Erhai	256.5 km^2; 10 m; 1978 m; whole year	2012	EC and ANN	1165	874 Apr–Nov	*Liu et al.* [2014]
Zige Tang Co	187 km^2; 38.9 m; 4560 m; ----	1958–1998	Penman method	925	747 Apr–Nov	*Li et al.* [2001]
Small lake adjacent to Nam Co	1 km^2; 7 m; 4730 m; Apr–Nov	2012–2013	EC and Bulk method	----	812 10 Apr to 10 Nov	This paper

[a] $\bar{E}$ is the total evaporation over the whole year; E indicates evaporation over specified months.
[b] Average value of 2012–2013 in *Lazhu et al.* [2016].

interpolated over by optimized models and then validated through observations; and the observations of energy budget components are relatively complete over the two ice-free periods. Even so, several uncertainties still exist. (1) Due to the lake's environment and complex underwater bathymetry, the heat storage in the water and heat transfer between water and sediments are heterogeneous. For example, the heat storage estimated from shallow observations does not represent the heat storage of the whole lake. The imbalance of the energy budget on daily and monthly scales reflected by our observations suggests heat transfer through mixing or vertical heat exchange through the water-sediment interface. Further, the footprints of our measurements of eddy fluxes, radiation, and water storage are not identical, and mismatches in these footprints will result in an apparent imbalance among energy budget components. However, such effects could be partly ameliorated for the whole ice-free period. (2) The eddy fluxes may be generally underestimated due to undetected large eddies [*Foken et al.*, 2006]. Vertical and horizontal advection may exist in the lake-land circulation, and this advection cannot be captured by EC instruments. Such effects may be strong for lakes with complex surrounding environments as in *Nordbo et al.* [2011] but should be relatively small for the homogeneous area surrounding the small lake examined in this study. (3) This small lake, which has no inflow and no outflow, should dry out given that evaporation exceeds precipitation. Therefore, some water must be supplied by groundwater. Such an influx of water will lead to an energy budget imbalance, and it needs to be quantified by further water balance analysis. (4) The B model will overestimate *LE* when stable atmospheric conditions dominate over the water surface [*Wang et al.*, 2015]. Although unstable and neutral atmospheric conditions dominate over this small lake, stable atmospheric conditions may occur occasionally.

3.3.2. Evaporation

Evaporation values from six high-altitude lakes are listed in Table 5, and the position of each lake is shown in Figure 1a. Evaporation from the small lake over the ice-free period (from 10 April through 10 November) is approximately 812 mm, which is larger than the climatological normal value for Nam Co (lake 2 in Figure 1a), which has an average evaporation of approximately 627 mm, as shown in Table 5 derived using the Flake model [*Lazhu et al.*, 2016], the complementary relationship method [*Ma et al.*, 2016], and bulk methods [*Shigenori et al.*, 2009; *Xu et al.*, 2009]. The larger evaporation may result from the larger water vapor pressure gradient caused by higher lake surface temperatures in the small and shallow lake than in the large and deep lake, as the former will have weaker wind-induced mixing and a shallower mixing layer depth. The differing duration of ice-cover periods is another factor that can explain evaporation differences. The evaporation from the small lake is also much larger than that of lake Ngoring (lake 4 in Figure 1a) [*Li et al.*, 2015], which has a value of 440 mm from June to November. In addition to lake Ngoring's large area and great depth, it also experiences smaller net radiation, which is another factor explaining why it experiences relatively small

evaporation compared with our results. Our result is much closer to the evaporation determined by EC and artificial neural network (ANN) methods in Erhai Lake (lake 5 in Figure 1a: Erhai Lake has an evaporation value of 874 mm [*Liu et al*., 2014]), bulk method-derived evaporation estimates from Yamdrok Yum Co (lake 1 in Figure 1a, which has an evaporation value of 830 mm [*Yu et al*., 2011]), and Penman method-derived evaporation from Zige Tang Co (lake 3 in Figure 1a, which has an evaporation value of 747 mm [*Li et al*., 2001]) over the same period. Climatic backgrounds (radiation, cloud cover, etc.), morphological characteristics (shape, depth, area, etc.), surrounding environments, and the type of simulation methods used (bulk methods, Penman methods, etc.) will introduce uncertainties into the reported evaporation values.

4. Conclusions

The environmental factors controlling turbulent flux and energy budget over temporal scales of half hourly, daily, and monthly were analyzed by using 2 years of EC, radiation, and water temperature profile measurements over the ice-free period of a small high-altitude lake on the Tibetan Plateau. After analyzing half-hourly lake-air turbulent flux data, a bulk aerodynamic transfer model is calibrated and used to interpolate turbulent flux values over periods when the measurements are inadequate or missing. Thus, continuous measurements over two ice-free periods are obtained for further daily and monthly analysis. The main results are summarized as follows: the optimized parameters from observations collected in 2012 are adequate for observations in 2013, and it suggests adequate of B model for interpolating over missing or inadequate data, with monthly mean biases of $-2.2 \pm 1.1\ \mathrm{W\,m^{-2}}$ in H and $11.2 \pm 3.7\ \mathrm{W\,m^{-2}}$ in LE. At half-hourly scales, wind speed shows an increasing trend in correlations with H from extremely unstable to neutral atmospheric conditions, while the contribution from temperature gradient is relatively stable ($R^2 = 0.4$). For LE, wind speed generally has a higher contribution, while water vapor gradient shows almost no correlation under near-neutral and neutral conditions. Generally, wind speed is most important at half-hourly scales, while temperature gradient and water vapor gradient are most important at daily and monthly scales. The evaporation over the small lake is approximately 812 mm, larger than that from Nam Co, and the energy budget over the entire ice-free period is generally closed, with an estimated EBC value of approximately 0.97.

Acknowledgments

This research has been funded by the Chinese Academy of Sciences (XDB03030201 and QYZDJ-SSW-DQC019), the National Natural Science Foundation of China (91337212, 41375009, and 41661144043), China Postdoctoral Science Foundation, "Hundred Talent Program" (Weiqiang Ma), and the EU-FP7 "CORE-CLIMAX" project (313085). The authors would like to thank Lang Zhang, Cunbo Han, and colleagues from Nam Co station, ITPCAS for installing and maintaining the measurement systems. The data used in this paper can be shared with the scientific public by emailing the corresponding author (wangbinbin@itpcas.ac.cn).

References

Alt, H., and M. Godau (1995), Computing the Fréchet distance between two polygal curves, *Int. J. Comput. Geom. Appl.*, *05*(01n02), 75–91, doi:10.1142/S0218195995000064.

Assouline, S., S. W. Tyler, J. Tanny, S. Cohen, E. Bou-Zeid, M. B. Parlange, and G. G. Katul (2008), Evaporation from three water bodies of different sizes and climates: Measurements and scaling analysis, *Adv. Water Resour.*, *31*(1), 160–172, doi:10.1016/j.advwatres.2007.07.003.

Biermann, T., W. Babel, W. Ma, X. Chen, E. Thiem, Y. Ma, and T. Foken (2013), Turbulent flux observations and modelling over a shallow lake and a wet grassland in the Nam Co basin, Tibetan Plateau, *Theor. Appl. Climatol.*, 1–16, doi:10.1007/s00704-013-0953-6.

Blanken, P. D., W. R. Rouse, A. D. Culf, C. Spence, L. D. Boudreau, J. N. Jasper, B. Kochtubajda, W. M. Schertzer, P. Marsh, and D. Verseghy (2000), Eddy covariance measurements of evaporation from Great Slave Lake, Northwest Territories, Canada, *Water Resour. Res.*, *36*, 1069–1077, doi:10.1029/1999WR900338.

Blanken, P. D., W. R. Rouse, and W. M. Schertzer (2003), Enhancement of evaporation from a large northern lake by the entrainment of warm, dry air, *J. Hydrometeorol.*, *4*(4), 680–693, doi:10.1175/1525-7541(2003)004<0680:eoefal>2.0.co;2.

Blanken, P. D., C. Spence, N. Hedstrom, and J. D. Lenters (2011), Evaporation from Lake Superior: 1. Physical controls and processes, *J. Great Lakes Res.*, *37*(4), 707–716, doi:10.1016/j.jglr.2011.08.009.

Brutsaert, W. (1982), Evaporation into the atmosphere: Theory, history, and applications, D. Reidel, Dordrecht, Netherlands.

Chen, B., X.-D. Xu, S. Yang, and W. Zhang (2012), On the origin and destination of atmospheric moisture and air mass over the Tibetan Plateau, *Theor. Appl. Climatol.*, *110*(3), 423–435, doi:10.1007/s00704-012-0641-y.

Dai, Y., T. Yao, X. Li, and F. Ping (2016), The impact of lake effects on the temporal and spatial distribution of precipitation in the Nam Co basin, Tibetan Plateau, *Quat. Int.*, doi:10.1016/j.quaint.2016.01.075.

Fairall, C. W., E. F. Bradley, J. S. Godfrey, G. A. Wick, J. B. Edson, and G. S. Young (1996), Cool-skin and warm-layer effects on sea surface temperature, *J. Geophys. Res.*, *101*, 1295–1308, doi:10.1029/95JC03190.

Foken, T., F. Wimmer, M. Mauder, C. Thomas, and C. Liebethal (2006), Some aspects of the energy balance closure problem, *Atmos. Chem. Phys.*, *6*, 4395–4402.

Gianniou, S. K., and V. Z. Antonopoulos (2007), Evaporation and energy budget in Lake Vegoritis, Greece, *J. Hydrol.*, *345*(3–4), 212–223, doi:10.1016/j.jhydrol.2007.08.007.

Granger, R. J., and N. Hedstrom (2011), Modelling hourly rates of evaporation from small lakes, *Hydrol. Earth Syst. Sci.*, *15*(1), 267–277, doi:10.5194/hess-15-267-2011.

Haginoya, S., H. Fujii, T. Kuwagata, J. Xu, Y. Ishigooka, S. Kang, and Y. Zhang (2009), Air-lake interaction features found in heat and water exchanges over Nam Co on the Tibetan Plateau, *Scie. Online Lett. Atmos.*, *5*, 172–175, doi:10.2151/sola.2009-044.

Heikinheimo, M., M. Kangas, T. Tourula, A. Venäläinen, and S. Tattari (1999), Momentum and heat fluxes over lakes Tämnaren and Råksjö determined by the bulk-aerodynamic and eddy-correlation methods, *Agr. Forest Meteorol.*, *98–99*, 521–534, doi:10.1016/S0168-1923(99)00121-5.

Lazhu, K., J. Yang, Y. Wang, Y. Lei, L. Chen, B. D. Zhu, and J. Qin (2016), Quantifying evaporation and its decadal change for Lake Nam Co, central Tibetan Plateau, *J. Geophys. Res. Atmos.*, *121*, 7578–7591, doi:10.1002/2015JD024523.

Li, W., S. Li, and P. Pu (2001), Estimates of plateau lake evaporation: A case study of Zige Tangco [in Chinese], *J. Lake Sci.*, *13*(3), 227–232.
Li, Z., S. Lyu, Y. Ao, L. Wen, L. Zhao, and S. Wang (2015), Long-term energy flux and radiation balance observations over Lake Ngoring, Tibetan Plateau, *Atmos. Res.*, *155*, 13–25, doi:10.1016/j.atmosres.2014.11.019.
Liu, H. Z., J. W. Feng, J. H. Sun, L. Wang, and A. L. Xu (2014), Eddy covariance measurements of water vapor and CO_2 fluxes above the Erhai lake [in Chinese], *Sci. Chin.: Earth Sci.*, *44*, 2527–2539, doi:10.1007/s11430-014-4828-1.
Liu, H., Y. Zhang, S. Liu, H. Jiang, L. Sheng, and Q. L. Williams (2009), Eddy covariance measurements of surface energy budget and evaporation in a cool season over southern open water in Mississippi, *J. Geophys. Res.*, *114*, D04110, doi:10.1029/2008JD010891.
Liu, H., Q. Zhang, and G. Dowler (2012), Environmental controls on the surface energy budget over a large southern inland water in the United States: An analysis of one-year eddy covariance flux data, *J. Hydrometeorol.*, *13*(6), 1893–1910, doi:10.1175/JHM-D-12-020.1.
Liu, J., S. Kang, T. Gong, and A. Lu (2010), Growth of a high-elevation large inland lake, associated with climate change and permafrost degradation in Tibet, *Hydrol. Earth Syst. Sci.*, *14*(3), 481–489, doi:10.5194/hess-14-481-2010.
Ma, N., J. Szilagyi, G.-Y. Niu, Y. Zhang, T. Zhang, B. Wang, and Y. Wu (2016), Evaporation variability of Nam Co Lake in the Tibetan Plateau and its role in recent rapid lake expansion, *J. Hydrol.*, *537*, 27–35, doi:10.1016/j.jhydrol.2016.03.030.
Ma, Y., et.al. (2014), Combining MODIS, AVHRR and in situ data for evapotranspiration estimation over heterogeneous landscape of the Tibetan Plateau, *Atmos. Chem. Phys.*, *14*, 1507–1515.
Mauder, M., and F. Thomas (2015), Eddy-covariance software TK3, *Zenodo*, doi:10.5281/zenodo.20349.
Nordbo, A., S. Launiainen, I. Mammarella, M. Leppäranta, J. Huotari, A. Ojala, and T. Vesala (2011), Long-term energy flux measurements and energy balance over a small boreal lake using eddy covariance technique, *J. Geophys. Res.*, *116*, D02119, doi:10.1029/2010JD014542.
Rosenberry, D. O., T. C. Winter, D. C. Buso, and G. E. Likens (2007), Comparison of 15 evaporation methods applied to a small mountain lake in the northeastern USA, *J. Hydrol.*, *340*(3–4), 149–166, doi:10.1016/j.jhydrol.2007.03.018.
Rouse, W. R., C. M. Oswald, J. Binyamin, P. D. Blanken, W. M. Schertzer, and C. Spence (2003), Interannual and seasonal variability of the surface energy balance and temperature of central Great Slave Lake, *J. Hydrometeorol.*, *4*, 720–730.
Rouse, W. R., C. J. Oswald, J. Binyamin, C. Spence, W. M. Schertzer, P. D. Blanken, N. Bussières, and C. R. Duguay (2005), The role of northern lakes in a regional energy balance, *J. Hydrometeorol.*, *6*(3), 291–305, doi:10.1175/JHM421.1.
Shigenori, H., F. Hideyuki, K. Tsuneo, and X. Jianqing (2009), Air-lake interaction features found in heat and water exchanges over Nam Co on the Tibetan Plateau, *SOLA*, *5*, 172–175.
Sugita, M., H. Ikura, A. Miyano, K. Yamamoto, and W. Zhongwang (2014), Evaporation from Lake Kasumigaura: Annual totals and variability in time and space, *Hydrol. Res. Lett.*, *8*(3), 103–107, doi:10.3178/hrl.8.103.
Tanny, J., S. Cohen, S. Assouline, F. Lange, A. Grava, D. Berger, B. Teltch, and M. B. Parlange (2008), Evaporation from a small water reservoir: Direct measurements and estimates, *J. Hydrol.*, *351*(1–2), 218–229, doi:10.1016/j.jhydrol.2007.12.012.
Venalainen, A., M. Frech, and M. Heikinheimo (1999), Comparison of latent and sensible heat fluxes over boreal lakes with concurrent fluxes over a forest: implications for regional averaging, *Agr. Forest Meteorol.*, *98–99*, 535–546.
Verburg, P., and J. P. Antenucci (2010), Persistent unstable atmospheric boundary layer enhances sensible and latent heat loss in a tropical great lake: Lake Tanganyika, *J. Geophys. Res.*, *115*, D11109, doi:10.1029/2009JD012839.
Wang, B., Y. Ma, X. Chen, W. Ma, Z. Su, and M. Menenti (2015), Observation and simulation of lake-air heat and water transfer processes in a high-altitude shallow lake on the Tibetan Plateau, *J. Geophys. Res. Atmos.*, *120*, 12,327–12,344, doi:10.1002/2015JD023863.
Xu, J., S. Yu, J. Liu, S. Haginoya, Y. Ishigooka, T. Kuwagata, M. Hara, and T. Yasunari (2009), The implication of heat and water balance changes in a lake basin on the Tibetan Plateau, *Hydrol. Res. Lett.*, *3*, 1–5.
Yang, K., H. Wu, J. Qin, C. Lin, W. Tang, and Y. Chen (2014), Recent climate changes over the Tibetan Plateau and their impacts on energy and water cycle: A review, *Global Planet. Change*, *112*, 79–91, doi:10.1016/j.gloplacha.2013.12.001.
Yao, H. X. (2009), Long-term study of lake evaporation and evaluation of seven estimation methods: Results from Dickie Lake, South-Central Ontario, Canada, *J. Water Resour. Prot.*, *1*(2), 59–77.
Yu, S., J. Liu, J. Xu, and H. Wang (2011), Evaporation and energy balance estimates over a large inland lake in the Tibet-Himalaya, *Environ. Earth Sci.*, *64*(4), 1169–1176.
Zhang, G., H. Xie, S. Kang, D. Yi, and S. F. Ackley (2011), Monitoring lake level changes on the Tibetan Plateau using ICESat altimetry data (2003–2009), *Remote Sens. Environ.*, *115*(7), 1733–1742, doi:10.1016/j.rse.2011.03.005.
Zhang, Q., and H. Liu (2014), Seasonal changes in physical processes controlling evaporation over inland water, *J. Geophys. Res. Atmos.*, *119*, 9779–9792, doi:10.1002/2014JD021797.
Zhu, L., M. Xie, and Y. Wu (2010), Quantitative analysis of lake area variations and the influence factors from 1971 to 2004 in the Nam Co basin of the Tibetan Plateau, *Chin. Sci. Bull.*, *55*(13), 1294–1303, doi:10.1007/s11434-010-0015-8.